Fusion of Sparse Reconstructions

William Meiniel
Telecom ParisTech,
Universite Paris-Saclay, France.
BioImage Analysis Unit,
Institut Pasteur, France.

Jean-Christophe Olivo-Marin
BioImage Analysis Unit,
Institut Pasteur, France.

Elsa D. Angelini
Telecom ParisTech,
Universite Paris-Saclay, France.
NIHR Imperial BRC,
ITMAT Data Science Group,
Imperial College London, UK.

***Abstract*—In this work, we present several variations of the fusion of sparsity-based reconstructions. The method exploits TV-sparsity to obtain multiple estimators of the original image, that are then aggregated using specific strategies. We tested the technique for denoising of microscopic images.**

I. Generation of multiple sparsity-based estimators

In the case of microscopic images, information concerning details of the structures is located in the high-frequency Fourier coefficients which are much more degraded by noise than the low-frequency coefficients which encode structural information of the objects inside the image [1].

We consider a dense low-pass sampling in the Fourier domain (selection of all the coefficients with frequency $\nu < \nu_c$), completed with a random sampling of high-frequency coefficients, with an overall sampling rate of $\tau \in [0, 1]$ (see [2]). Denote by Φ_k the corresponding sampling matrix.

From the single noisy observation y, we generate R sets of partial estimators $\hat{x}_k$, solving the following Total Variation-based convex optimization problems:

$$\hat{x}_k = \underset{x \in \mathbb{R}^N}{\arg\min} \|x\|_{\mathrm{TV}} \quad \text{s.t.} \quad \|\Phi_k x - y_k\|_2 \leq \epsilon \tag{1}$$

where $y_k = \Phi_k y$ and ϵ is a noise-dependent parameter defined in [3]. In this equation, σ_n represents the standard deviation of the additive Gaussian component of the noise, and γ_ϵ is a gain that we introduce to handle specific image types.

We can immediately define the following pixel-wise statistics over the R reconstructions:

$$\hat{x}_{\mathrm{mean}}(s) = \frac{1}{R}\sum_{k=1}^{R} \hat{x}_k(s)$$

$$\hat{x}_{\mathrm{var}}(s) = \frac{1}{R-1}\sum_{k=1}^{R} (\hat{x}_k(s) - \hat{x}_{\mathrm{mean}}(s))^2$$

where $\hat{x}_{\mathrm{var}}$ is called the variance map.

II. Fusion of sparse reconstructions

Fusion of partial operators is tested for image enhancement and denoising. We test three fusion operators based in space or Fourier domain, each of them pursuing different purposes.

A. Linear Weighted Combination with Variance map

As used in [4], the Linear Weighted Combination (LWC) fusion technique combines simple averaging of the estimators with spatial localization of reconstructions given by the variance map. This estimator is defined as:

$$\hat{x}_{LWC}(s) = \sqrt{\hat{x}_{\mathrm{var}}(s)} \circ \mathcal{H}\left(y(s)\right) + \left(1 - \sqrt{\hat{x}_{\mathrm{var}}(s)}\right) \times \hat{x}_{\mathrm{mean}}(s) \tag{2}$$

where y is the noisy observation, and $\mathcal{H}$ is a local filter (e.g. median filter, edge-enhancement filter, etc.). This fusion operator bears some similarity with the Lee filter [5].

B. Exponentially Weighted Aggregate

In [6], Exponentially Weighted Aggregate (EWA) is an aggregation method that was designed to reach optimal average risk, in the context of non-parametric statistical regression, and has been adapted to image denoising in [7]. The EWA aggregator is defined as:

$$\forall s \in \Omega, \quad \hat{x}_{\mathrm{EWA}}(s) = \sum_{k=1}^{R} \theta_k(s)\hat{x}_k(s)$$

with

$$\theta_k(s) = \frac{\exp(-|r_k(s)|/\beta)\pi_k(s)}{\sum_{i=1}^{R}\exp(-|r_i(s)|/\beta)\pi_i(s)}$$

where $\beta > 0$, $\{\pi_i(s)\}_{i=1,.,R}$ is drafted from a probability distribution function $\pi(s)$. In our work we defined π as a uniform random distribution and $\beta = 0.01$. Note that $r_k(s) = \|y(s) - \hat{x}_k(s)\|_2^2 - \sigma_n^2$ is the risk of the estimator $\hat{x}_k$ at pixel s, assuming a zero-mean additive white Gaussian noise with standard deviation σ_n.

C. Fourier Burst Accumulation

In [8], the authors propose an image deblurring method based on Fourier burst accumulation of multiple blurry acquisitions. Adapting this method to our context leads to a final estimator that has been optimized in the Fourier domain. Formally, the FBA aggregator is defined as:

$$\forall s \in \Omega, \quad \hat{x}_{\mathrm{FBA}}(s) = \mathcal{F}^{-1}\left(\sum_{k=1}^{R} w_k(\zeta) \circ \mathcal{F}(\hat{x}_k)(\zeta)\right)(s), \tag{3}$$

$$w_k(\zeta) = \frac{|\mathcal{F}(\hat{x}_k)(\zeta)|^p}{\sum_{l=1}^{R}|\mathcal{F}(\hat{x}_l)(\zeta)|^p} \tag{4}$$

where p is a non-negative integer, $\mathcal{F}$ represents the Fourier transform operator and ζ the frequency index. The parameter p emphasizes the predominance of the highest Fourier coefficient value. In our work, we empirically identified $p = 15$ as the value leading to optimal results.

III. Results

We display on Fig.1 the denoising performance of our three methods, and compare the performance with the state-of-the-art BM3D denoising method [9]. The first tested image is a synthetic cell image [10], composed of a constant back-ground and several cells (cytoplasm, nucleus and intra-cellular objects), and the second one is a HeLa cell image obtained in fluorescence microscopy. Both images are corrupted with a realistic mixed Poisson-Gaussian noise with variance $\sigma_n = 0.1$.

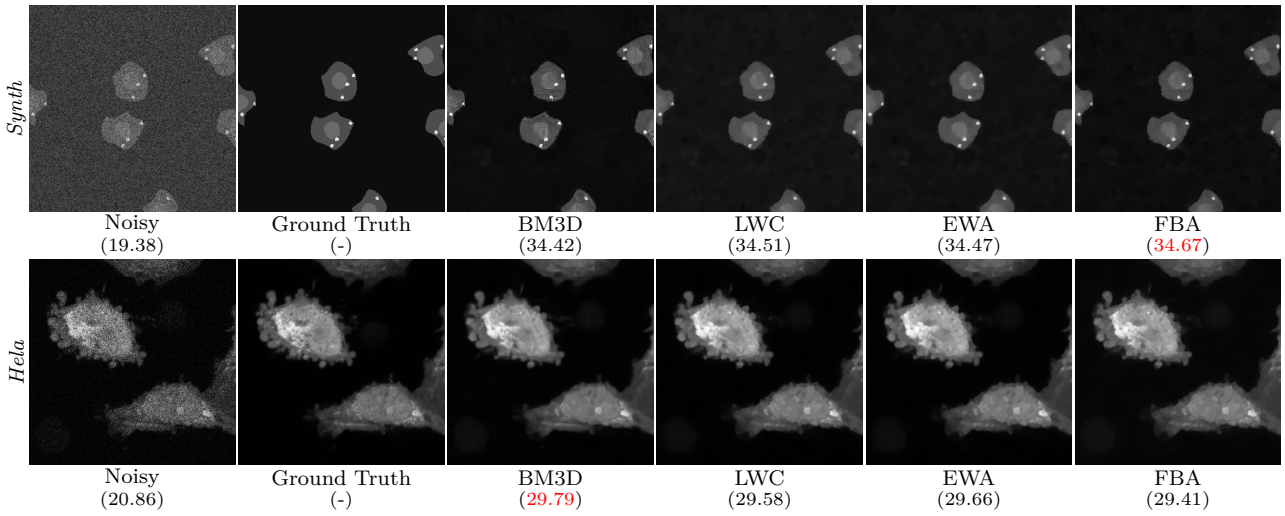

Fig. 1: **Application of the FSR methods to the denoising of microscopic images. Results are compared with the state-of-the-art method BM3D, and we display the PSNR measure of the reconstructions.**

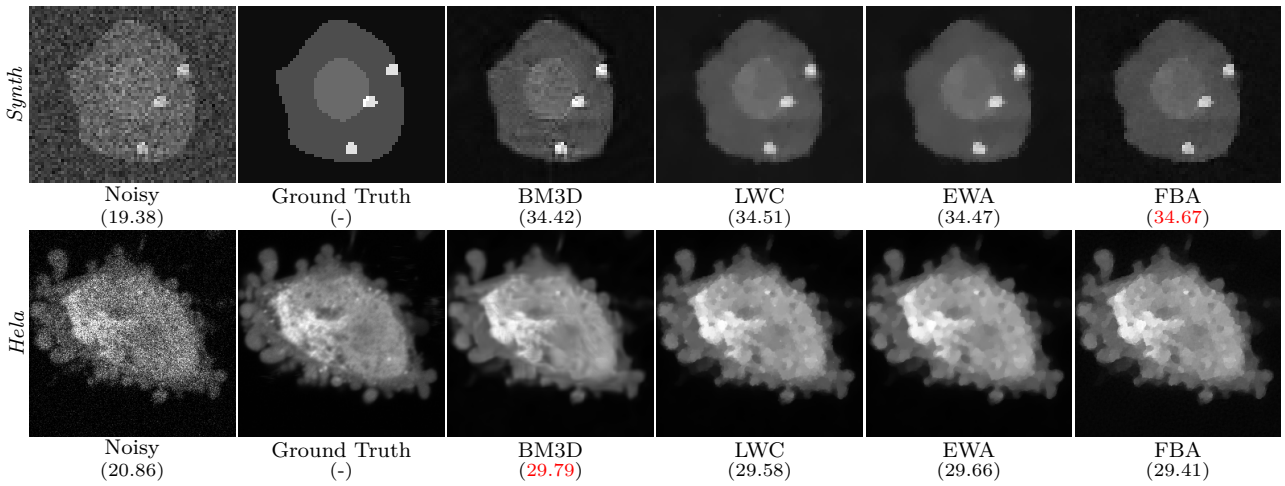

Fig. 2: **Zoom on the results displayed on Fig 1. On the *Synth* image, the LWC and EWA methods reconstruct well the flat areas. The FBA method preserves the high contrast of the small objects. On the *Hela* image, the BM3D method gives a smoother result.**

The proposed techniques show similar performance with the BM3D technique in terms of PSNR measure, while preventing the artifacts due to the wavelet processing, visible mostly on the synthetic image.

References

[1] Z. Wang and G. Arce, "Variable density compressed image sampling," *IEEE Transactions on Image Processing*, vol. 19, no. 1, pp. 264–270, 2010.

[2] Y.-C. Kim, S. Narayanan, and K. Nayak, "Accelerated three-dimensional upper airway MRI using compressed sensing," *Magnetic Resonance in Medicine*, vol. 61, no. 6, pp. 1434–1440, 2009.

[3] S. Becker, J. Bobin, and E. Candès, "Nesta: A fast and accurate first-order method for sparse recovery," *Journal on Imaging Sciences*, vol. 4, no. 1, pp. 1–39, 2011.

[4] W. Meiniel, E. Angelini, and J.-C. Olivo-Marin, "Image denoising by adaptive compressed sensing reconstructions and fusions," in *SPIE Optical Engineering+ Applications*. International Society for Optics and Photonics, 2015, pp. 95 970X–95 970X.

[5] J.-S. Lee, "Digital image enhancement and noise filtering by use of local statistics," *IEEE Transactions on Pattern Analysis and Machine Intelligence*, no. 2, pp. 165–168, 1980.

[6] A. Dalalyan and A. Tsybakov, "Aggregation by exponential weighting, sharp PAC-Bayesian bounds and sparsity," *Machine Learning*, vol. 72, no. 1-2, pp. 39–61, 2008.

[7] C. Kervrann, "PEWA: Patch-based exponentially weighted aggregation for image denoising," in *Advances in Neural Information Processing Systems*, 2014, pp. 2150–2158.

[8] M. Delbracio and G. Sapiro, "Hand-held video deblurring via efficient fourier aggregation," *IEEE Transactions on Computational Imaging*, vol. 1, no. 4, pp. 270–283, 2015.

[9] K. Dabov, A. Foi, V. Katkovnik, and K. Egiazarian, "Image denoising by sparse 3-D transform-domain collaborative filtering," *IEEE Transactions on Image Processing (TIP)*, vol. 16, no. 8, pp. 2080–2095, 2007.

[10] P. Ruusuvuori, A. Lehmussola, J. Selinummi, T. Rajala, H. Huttunen, and O. Yli-Harja, "Benchmark set of synthetic images for validating cell image analysis algorithms," in *IEEE European Signal Processing Conference (EUSIPCO)*, 2008, pp. 1–5.